



Phase-controlled microwave synthesis of pure monoclinic BiVO₄ nanoparticles for photocatalytic dye degradation

Kanlaya Pingmuang^{a,b}, Andrew Nattestad^b, Wiyong Kangwansupamonkon^c, Gordon G. Wallace^b, Sukon Phanichphant^{a,*}, Jun Chen^{b,*}

^a Department of Chemistry and Materials Science Research Center, Faculty of Science, Chiang Mai University, 239 Huay Kaew Road, Muang District, Chiang Mai 50200, Thailand

^b ARC Centre of Excellence for Electromaterials Science, Intelligent Polymer Research Institute, Australian Institute of Innovative Materials, Innovation Campus, University of Wollongong, Fairy Meadow, NSW 2519, Australia

^c National Nanotechnology Center, Thailand, 130 Thailand Science Park, Paholyothin Road, Pathum Thani 12120, Thailand

ARTICLE INFO

Article history:

Received 29 July 2015

Received in revised form

23 September 2015

Accepted 29 September 2015

Keywords:

Phase-control

Microwave synthesis

BiVO₄

Photocatalysis

Dye degradation

ABSTRACT

Pure monoclinic bismuth vanadate (BiVO₄) nanoparticles were successfully prepared using a single step, pH-controlled, microwave approach. This simple, fast, synthesis is shown to be an industrially viable, low temperature ($\leq 90^\circ\text{C}$, non-vacuum) and environmentally benign alternate to other approaches. The parameters of the microwave synthesis protocol, including pH, temperature, and reaction time, were varied to control morphology and crystal phase. Optimal synthesis conditions for photocatalytic degradation of Rhodamine B (RhB) were determined and this material was compared against state-of-the art samples produced by more conventional methods, revealing very similar performances.

© 2015 Elsevier Ltd. All rights reserved.

1. Introduction

It has been well-documented that monoclinic BiVO₄ displays much better photocatalytic performance than that of other crystal phases under visible light irradiation. Various synthetic methods, such as solid-state reactions [1], precipitation reactions [1,2], sol-gel processes [3], and hydrothermal methods [4,5] have been employed to prepare BiVO₄ particles. In most of these methods (apart from hydrothermal), a high temperature treatment is required to facilitate good crystallinity. Hydrothermal processes also offer an advantage in that the crystal structure, size and particle morphology of BiVO₄ can be controlled by adjusting the temperature in the autoclave reactor and/or the precursor chemistry. The preparation of crystalline BiVO₄ nanoparticles through hydrothermal methods however has some disadvantages such as (1) requiring high pressure, (2) being limited to batch processing (typical using a Teflon-lined stainless-steel autoclave), (3) the difficulty in achieving uniform particle sizes, (4) requiring long reaction times, and (5) difficulties in monitoring the reaction in progress.

Recently, there have been a few reports on BiVO₄ powder synthesised by a modified hydrothermal method using a Teflon-lined

stainless-steel autoclave as the reactor, heated by microwave irradiation [7]. Li et al. synthesised monoclinic BiVO₄ microspheres from aqueous Bi(NO₃)₃ and NH₄VO₃ solutions under microwave irradiation (300 W) at 180 °C for 3 h [8]. The resultant monoclinic BiVO₄ consisted of microspheres, themselves composed of small particles and randomly oriented nanosheets. Zhu et al. also synthesised decahedral BiVO₄ particles with Bi(NO₃)₃ and NH₄VO₃ as precursors and Tween-80 as a template, by a combined hydrothermal-microwave method [8]. It was found that the synthesised BiVO₄ was microstructured and monoclinic. Recently, Tan et al. synthesised BiVO₄ powders with hierarchical structures using another combined hydrothermal-microwave method, from precursor solutions of Bi(NO₃)₃·5H₂O and NH₄VO₃, at various pH values. These were heated to 200 °C for 40 min, leading to different crystal phases and morphologies [10]. Furthermore, Zhang et al. also reported that monoclinic BiVO₄ micro/nanostructures were synthesised by a rapid microwave-assisted method, a combined microwave and ultrasonication technique [6]. These results showed that the solvents (diethylene glycol and deionized water) and the pH had a significant influence on morphology, size and crystallinity.

In the aforementioned works, the use of a microwave-assistant heating step has been employed to significantly reduce processing time and enhance product purity compared to when conventional heat sources are used. It has been observed that while microwave irradiation provides uniform heating in the reactor, this energy is

* Corresponding authors.

E-mail address: junc@uow.edu.au (J. Chen).

more likely to be transferred to ionic species (such as precursor salts) [11]. These ionic species oscillate and quickly collide with their neighbouring molecules allowing an enhanced reaction rate. This is modelled according to an Arrhenius equation as follows, ($k = A_{exp} (-E_a/RT)$) [11b], where microwave energy increases the pre-exponential factor (A_{exp}) or the activation energy (E_a) associated to the reaction rate (k) at temperature (T) and gas constant (R).

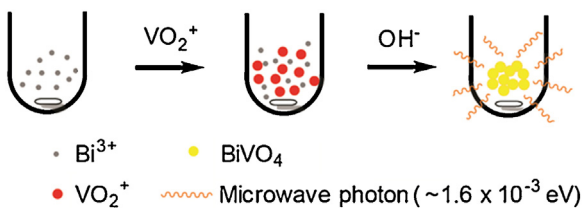
The above methods still use high temperatures, which necessarily require pressurisation when using aqueous solutions and as such limit processes to being batch. Thus, efficient, simple, and low temperature processing is required to synthesise high quality BiVO₄ powders. In this research, a single-step pH-dependent microwave-only approach, with low irradiation power (<300 W) was developed to achieve phase-controlled synthesis of pure-monoclinic BiVO₄ nanoparticles. The physical properties of the BiVO₄ powders along with those produced by conventional hydrothermal method were compared and investigated through monitoring Rhodamine B (RhB) degradation under simulated solar illumination (AM1.5G, 1 sun equivalent).

2. Experimental

2.1. Synthesis of BiVO₄ powders

BiVO₄ nanoparticles were prepared by an aqueous-microwave synthesis using an Advanced Microwave System (APEX, China) which allows for control over reaction power, time and temperature with an AC frequency of 50 kHz. Bismuth nitrate pentahydrate (Bi(NO₃)₃·5H₂O, 98%, Sigma-Aldrich) and Ammonium metavanadate (NH₃VO₄, 99%, Sigma-Aldrich) were used as bismuth and vanadium precursors, respectively. Firstly, 0.125 M each of precursors were separately prepared by dissolving Bi(NO₃)₃·5H₂O or NH₃VO₄ in 1 M nitric acid aqueous solution. A schematic diagram for the synthesis of BiVO₄ nanoparticles is shown in **Scheme 1**. Briefly, the bismuth nitrate solution was transferred to a reactor (Quartz glass, 100 mL) and heated up to 90 °C (<300 W) by microwave irradiation. The vanadium precursor was then added into this bismuth solution. Subsequently, a 3 M ammonium hydroxide solution was slowly added until the desired pH was attained (1, 3, 5, 7, 9 or 12). The solution was kept stirring under maximum power of 300 W microwave irradiation with different temperature (60 °C or 90 °C) and holding time (5, 15, 30 or 60 min), after which it was allowed to cool to room temperature. Then the resultant precipitate was washed with deionized water, centrifuged and dried at 60 °C for 12 h. BiVO₄ powders were also synthesised by hydrothermal and precipitation methods from the same precursors and reaction temperature for comparative purposes. Additionally, BiVO₄ was synthesised by a hydrothermal method at 120 °C for 6 h as reported previously [18].

The following format has been used “MM-tt-TT-pH” where “MM” represents the method (MW=microwave, HT=hydrothermal, PC= precipitate), “tt” represents the reaction time (in minutes), “TT” the temperature (°C) and “pH” the precursor pH value.



Scheme 1. Schematic illustration of microwave synthesis of BiVO₄ nanoparticles.

2.2. Material characterizations

The crystal structures of the BiVO₄ powders were determined by an X-ray diffraction (GBC MMA XRD) with CuK α radiation ($\lambda = 0.154$ nm) in the range of 15–70°. The morphologies of BiVO₄ powders were investigated by scanning electron microscope (SEM, JEOL JSM-7500FA) and transmission electron microscopy (TEM, JEOL JEM-2010). Light absorption of the BiVO₄ across the UV-visible spectrum (300–800 nm) was investigated with a Shimadzu UV-3600 spectrophotometer, with an integrating sphere attachment (Shimadzu ISR-3100). A Quantachrome ASiQwin-nitrogen gas adsorption system was used to determine the surface area of the catalysts. In order to investigate the flat band potential (E_{fb}), Mott-Schottky analysis was carried out in a three-electrode system with 0.5 M Na₂SO₄ solution at frequency 1 kHz. The BiVO₄ powders synthesised by microwave and hydrothermal methods were coated FTO as working electrode, a Pt-wire as counter electrode, and Ag/AgCl as reference electrode.

2.3. Photocatalytic degradation of RhB dyes

The photocatalytic activities of the BiVO₄ powders towards the degradation of RhB (25 μ M) were studied under the illumination of AM 1.5 G one sun (100 mW cm⁻²). Photocatalyst powder (catalyst loading ~0.01 g per 20 mL of dye solution) were put in a reactor of dye solution and kept under stirring. Prior to irradiation, the catalyst was left overnight in the dye solution in order to attain an adsorption/desorption equilibrium. At irradiation time intervals of 30 min, the dye solution was collected the absorption measured using a Shimadzu UV-1601 spectrophotometer and returned to the reactor (<10 min intermission).

3. Results and discussion

The first parameter optimised for microwave synthesis was the solution pH. An aqueous solution of ammonium hydroxide was employed to adjust the pH values to 1, 3, 5, 7, 9 or 12, in order to produce MW-60-90-1, MW-60-90-3, MW-60-90-5, MW-60-90-7, MW-60-90-9 and MW-60-90-12, respectively. These reactions were all completed at a temperature of 90 °C (>300 W) with a duration of 60 min. The temperature for the microwave synthesis was set to 90 °C to avoid boiling the aqueous solutions.

The morphologies of the microwave synthesised BiVO₄ powders obtained at different solution pH were investigated by SEM (**Fig. 1**). In **Fig. 1(a)**, the SEM image of the MW-60-90-1 sample shows BiVO₄ microspheres composed of irregular particles (~50 nm) and some irregular polyhedra. The obtained microspheres had an average diameter of 3.8 μ m, while the smooth surfaced polyhedra were ~1.5 μ m.

As shown in **Fig. 1(b)**, the morphology of the MW-60-90-3 sample was predominantly large (~300 nm) plates with rough surfaces. Given that analysis of the XRD patterns suggested the crystal size to be ~60 nm it can be assumed that each of these is comprised of a number of highly aggregated, crystals. Meanwhile, the aggregates in MW-60-90-5, MW-60-90-7, MW-60-90-9 and MW-60-90-12 were quite different from those of MW-60-90-1 and MW-60-90-3. The MW-60-90-5 sample (**Fig. 1(c)**) contained mixture of large and small spherical particles with average size of 120 nm and 50 nm, respectively. Small spherical particles, in the range of 50–80 nm, are also seen in the SEM images of both MW-60-90-7 (**Fig. 1(d)**) and MW-60-90-9 (**Fig. 1(e)**). However, the average particle size of MW-60-90-12 (**Fig. 1(f)**) was once again quite large. Here it can clearly be seen that these particles are aggregates, composed larger irregular particles with diameters of about 250 nm.

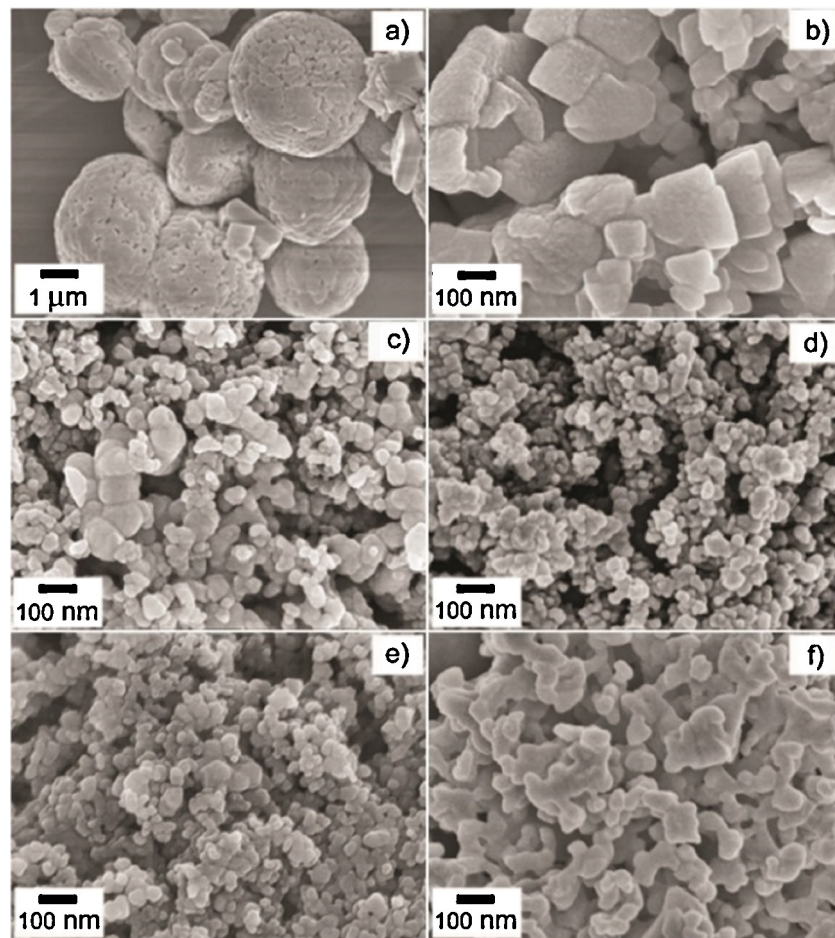


Fig. 1. SEM images of BiVO_4 powders synthesised by the microwave method as a function of pH values: (a) MW-60-90-1, (b) MW-60-90-3, (c) MW-60-90-5, (d) MW-60-90-7, (e) MW-60-90-9 and (f) MW-60-90-12 at 90°C ($>300\text{ W}$) for 60 min.

The crystal structures of the BiVO_4 particles synthesised by this microwave method, using precursors of different pH values, were investigated by XRD as shown in Fig. 2. The diffraction peaks of monoclinic BiVO_4 were located at $2\theta = 28.8^\circ$, 30.6° , 34.5° , 35.2° ,

39.8° , and 42.5° , corresponding to (112), (004), (200), (020), (211), and (015) planes of monoclinic BiVO_4 (JCPDS No. 75-1866, space group: $I2/b$, unit cell parameters: $a = 5.194\text{ \AA}$, $b = 5.090\text{ \AA}$, $c = 11.697\text{ \AA}$, $\gamma = 90.39^\circ$), respectively. This was observed as the main structure for all of the as-synthesised BiVO_4 samples. According to the XRD patterns in Fig. 2, both MW-60-90-7 and MW-60-90-9 samples exhibited a single phase of monoclinic BiVO_4 . While all three samples obtained from lower pH precursors (MW-60-90-1, MW-60-90-3 and MW-60-90-5) showed a mixture of tetragonal (JCPDS no. 14-0133, space group: $I41/amd$, unit cell parameters: $a = 7.300\text{ \AA}$, $c = 6.457\text{ \AA}$) and monoclinic phases, with a trend of the increased monoclinic phase with higher pH value. For the MW-60-90-12 sample, no signals of crystalline diffraction peaks were observed in the XRD pattern, indicating an amorphous material. The volume percentage of the monoclinic phase and average crystalline size (determined by Scherrer equation) of the BiVO_4 powder are summarised in Table S1. It was found that under acidic conditions mixed phases of monoclinic and tetragonal BiVO_4 with coarse structure was produced. The crystallinity of monoclinic BiVO_4 decreased and become amorphous with strongly basic conditions (pH more than 9).

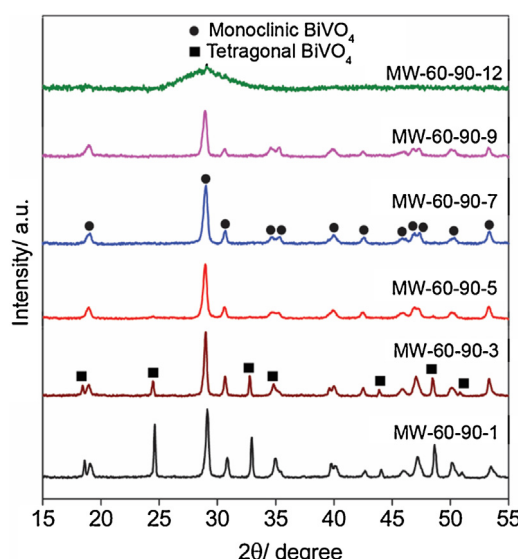


Fig. 2. XRD patterns of BiVO_4 powders synthesised by the microwave method at 90°C ($>300\text{ W}$) for 60 min as a function of pH values.

Raman spectroscopy provided further information about the local structure in the BiVO_4 powder, as shown in Fig. 3. The Raman bands at 320 , 367 , 637 , and 820 cm^{-1} , observed for each of the BiVO_4 samples, are characteristic of monoclinic BiVO_4 , similarly to reports by Gotić et al. [12] and Zhang et al. [13]. The Raman band at 210 cm^{-1} could be assigned to the external modes (rotation/translation) of BiVO_4 , while the bands at 320 and 367 cm^{-1}

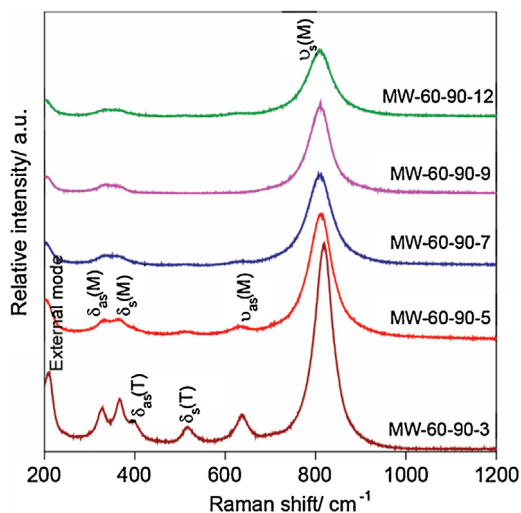


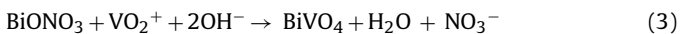
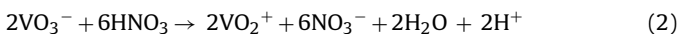
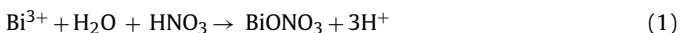
Fig. 3. Raman spectra of BiVO_4 powders synthesised by the microwave method at 90°C ($>300\text{ W}$) for 60 min for various precursor pH values.

were attributed to the asymmetric and symmetric V–O bending modes of the VO_4 tetrahedron, respectively. The bands at 637 and 820 cm^{-1} were ascribed to asymmetric and symmetric V–O stretching modes, respectively.

For MW-60-90-5, not only were the Raman bands of monoclinic BiVO_4 observed, but also three bands of tetragonal BiVO_4 , at 398 , 517 and 831 cm^{-1} . The bands at 398 and 517 cm^{-1} were attributed to the antisymmetric and symmetric V–O bending modes, respectively as reported by Sun et al. [14]. The 831 cm^{-1} band of tetragonal BiVO_4 overlapped with the main band of monoclinic BiVO_4 at around 820 cm^{-1} . In the measured samples this peak was observed to shift between the two values as the two peaks were not able to be deconvoluted. The peak at 831 cm^{-1} could be described as the symmetric V–O stretching mode, which was also reported by Zhang et al. [13]. Moreover, it was observed that the intensity of the Raman bands for the mixed phases of tetragonal and monoclinic BiVO_4 (MW-60-90-3 and MW-60-90-5) were much stronger than those of the single phase of monoclinic BiVO_4 (MW-60-90-7, MW-60-90-9 and MW-60-90-12) corresponding with the increase of the percentage of the monoclinic phase.

In comparison to XRD results (Fig. 2), it could be seen that Raman spectroscopy is more sensitive to the presence of tetragonal phase BiVO_4 than the monoclinic phase [14].

From XRD, Raman and SEM results, it is observed that phase-control of BiVO_4 powders, along with control over crystal size and shape is obtained by adjusting the pH value of precursor solution. In this one-pot microwave reaction, the growth mechanism of BiVO_4 nanoparticles can be explained by the amount of nuclei generated, which is pH-dependent (controlled by addition of ammonium hydroxide solution) [11a]. The proposed mechanism is presented below as Eqs. (1)–(3) [10,12].



When the precursor solutions were initially mixed together, no precipitate was observed. As NH_4OH was added to the mixture (to give a final pH of 1, 3, 5, 7, 9 or 12) BiVO_4 precipitates under microwave irradiation. In acidic conditions, the rate of reaction is slow, producing large particles with high crystallinity. These results are similar to those reported by Tan et al. [10], however, the micro-polyhedra and spheres become loose micro-plates at pH 3 or small spherical particles at pH higher than 3. As shown in Table S1, not

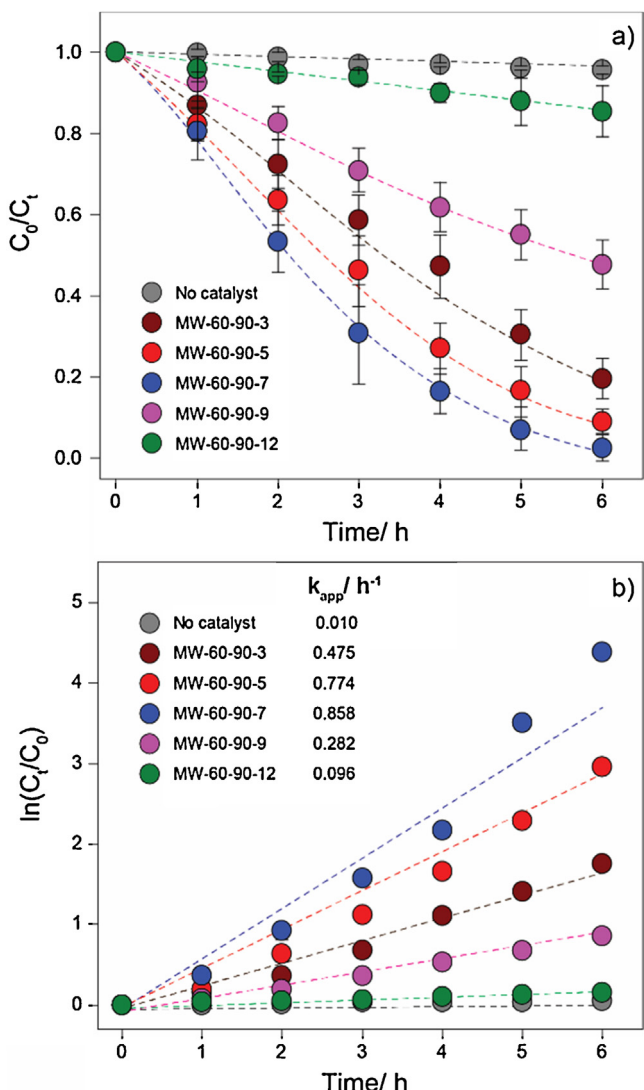


Fig. 4. (a) Photocatalytic activity and (b) kinetics ($\ln(C_0/C_t)$ vs. t) for RhB degradation with BiVO_4 powders produced with different pH value precursors.

only does the average particle size decrease, but so does crystalline size. This trend continues with an increase in pH, due to an increase in the nucleation rate and hence smaller crystal and particle sizes.

Amorphous structures are obtained at pH 12. It is assumed that $\text{Bi}(\text{OH})_3$ formation is favoured with highly basic conditions, thus, the synthesised BiVO_4 at pH 7 appeared to be optimal for the formation of monoclinic phase and nano-size particles under the microwave conditions tested. A schematic diagram for the synthesis of BiVO_4 nanoparticles is shown in Scheme 1.

RhB dye in aqueous solution was chosen as a model pollutant dye to study the photocatalytic activities of the microwave synthesised by BiVO_4 . Before solar irradiation, dye solution with catalyst powder was kept overnight in the dark in order to attain an adsorption/desorption equilibrium and to study the adsorption of the dyes on the catalyst surface. Fig. 4(a) shows photocatalytic degradation of RhB under simulated solar irradiation of the BiVO_4 powders as a function of time, along with a control (without photocatalyst). As expected, the degradation of RhB dye appears to show logarithmic relationship with respect to time. Thus, the photocatalytic degradation rate of RhB is fitted to the Langmuir–Hinshelwood (LH) model, using pseudo-first order kinetics ($\ln C_t/C_0 = k_{app}t$, where k_{app} is pseudo-first order rate constant) as presented in Fig. 4(b) [15,16]. The apparent rate constants are also presented in Table S1.

It was found that high crystallinity of the monoclinic structure and surface areas of the catalyst powders, calculated by using BET results (**Table S1**), were a strong determining factor for high photocatalytic activity. The MW-60-90-7 sample provided the highest photodegradation rate of 0.830 h^{-1} .

As further steps of optimisation, the effects of the reaction time and temperature on morphology, crystallinity and photocatalytic ability were studied. **Fig. S1** highlights that, irrespective of reaction time, the morphology of the BiVO₄ products produced are similarly, with irregular particles in the range of 80–120 nm.

XRD results, however, reveal more marked differences in crystallinity and phase purity. This also provides additional information about the manner in which monoclinic BiVO₄ is formed. The product of the short reaction time is a mixture of the monoclinic and tetragonal phases along with a substantial portion of amorphous material. With 15 min processing this amorphous material is no longer observed, giving way to more of the both the monoclinic and tetragonal phases. From 30 min onward there is a notable decrease in the quantity of tetragonal BiVO₄, however it is not until 60 min

that the material can be considered phase pure. The percentages of monoclinic BiVO₄ in these samples are reported in **Table S2**. With regard to their photocatalytic properties, the 60 min irradiated sample showed the best performance, this could be expected since this material was pure monoclinic BiVO₄ with small particle size.

The influence of different temperature (25 °C (RT), 60 °C, and 90 °C) was also studied with a fixed pH of 7 and reaction time of 60 min, as shown in **Fig. S2**. It was found that the reaction temperature employed for microwave synthesis of BiVO₄ has a minor effect on morphology and crystallinity. However, the BiVO₄ sample synthesised at temperature of 90 °C showed higher photocatalytic activity than 60 °C due to its higher crystallinity of monoclinic phase (**Table S3**). Control experiments, conducted at room temperature (25 °C) (PC-60-25-7) indicated that the crystalline BiVO₄ (**Fig. S2d**) could not form without microwave treatment, as the XRD of sample PC-60-25-7 only showed amorphous phase structure. As such, the optimum pH, reaction time and temperature for microwave synthesis of BiVO₄ were determined to be 7, 60 min and

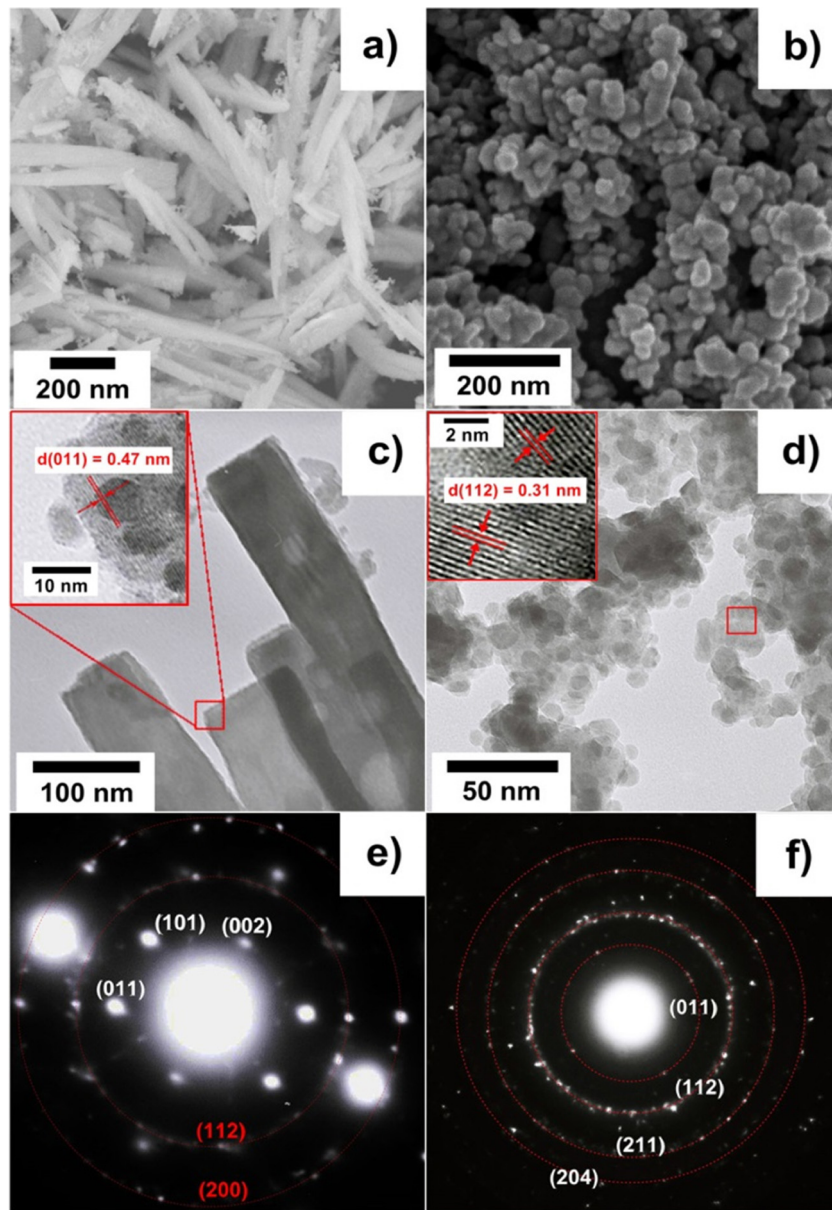


Fig. 5. (a) and (b) Typical SEM images; (c) and (d) TEM images; and (e) and (f) its SAED of synthesised BiVO₄ powders, HT-360-120-7 and MW-60-90-7, respectively.

90 °C, respectively. MW-60-90-7 provided single phase of monoclinic BiVO₄ with small spherical particles and high specific surface area, leading to a high photocatalytic degradation of RhB dye under solar irradiation.

To compare the photocatalytic performance of these novel materials against a previous reported high performance system of the photocatalytic behaviour of MW-60-90-7 was compared against BiVO₄ samples prepared by a hydrothermal method (HT-360-120-7) [17] under identical conditions, which is regarded to be state-of-the-art for this application.

The morphologies of HT-360-120-7 and MW-60-90-7 samples were compared, using SEM and TEM, as presented in Fig. 5. It was found that these are radically different with HT-360-120-7 primarily comprised of rod-like particles, about 100 nm in width and 3 μm in length (Fig. 5(a) and (c)). Lattice fringes of the samples are observed with spacings of 0.47 nm for the MW-60-90-7 (inset Fig. 5(c)) and 0.31 nm for HT-360-120-7 (inset Fig. 5(d)), which corresponded with the (0 1 1) and (1 1 2) lattice planes of monoclinic BiVO₄, respectively. These results confirm that the rod-like BiVO₄ (HT-360-120-7) grows in the (0 1 1) plane, corresponding high XRD relative intensities of (0 1 1) and (1 1 2) as calculated in Table S1. This agrees well with the results reported by Obregón et al. [4b] and Tan et al. [10]. Similarly, it can also be noted that MW-60-90-3 (Fig. 1(b)) showed large BiVO₄ plate morphology and provided a highly relative intensity of (0 0 4)/(1 1 2) (Table S1) [4b]. Thus, it could be concluded that growth in the (0 1 1) and (0 0 4) directions are associated with the rod-like and plate-like morphologies of monoclinic BiVO₄, respectively. Spherical growth appears to provide similar relative intensities in both planes as seen in the MW-60-90-7.

Furthermore, the corresponding SAED patterns (Fig. 5(e) and (f)) of the HRTEM images confirmed that all synthesised BiVO₄ samples had polycrystalline monoclinic structure, which is in agreement with XRD results as shown in Fig. 6(a). The percentage of monoclinic phase and calculated crystalline size of them also are presented in Table S4. The high crystallinity of both samples led to their high photocatalytic efficiencies as shown in Fig. 6(b).

MW-60-90-7 and HT-360-120-7, exhibited degradation rates of 0.830 h⁻¹ and 0.811 h⁻¹, respectively. MW-60-90-7 has a larger surface area providing a larger number of reaction interfaces leading to a higher photocatalytic activity than the HT-360-120-7. To better understand the reason for the superior performance of the microwave synthesised sample, XRD patterns of samples produced by hydrothermal (HT-60-90-7) methods, using the same experimental conditions (same precursors, pH 7, temperature of 90 °C and 60 min reaction time) were studied and compared as shown in (Fig. S3). While MW-60-90-7 sample was clearly monoclinic, HT-60-90-7 remained amorphous. This could be explained by the microwave energy being applied directly to ions in the solution providing a higher probability of collision and subsequent reaction, which allows for enhanced reaction rates [10].

The optical and electronic properties of the two BiVO₄ samples were investigated by UV-vis diffuse reflectance spectroscopy and the conduction band edges estimated from Mott–Schottky experiments. For the Mott–Schottky analysis, the MW-60-90-7 and HT-360-120-7 were fabricated on a fluorine doped tin oxide (FTO) substrate and annealing at 380 °C for 48 h to produce a condensed and stable electrode. This was necessary to avoid the FTO response being observed. The phase structure of both electrodes after annealing was monoclinic BiVO₄ (Fig. S4) which was similar to that of the powers (Fig. 6(a)). Mott–Schottky experiments were conducted in 0.5 M Na₂SO₄ solution (pH 5.8) at frequency 1 kHz, using a three electrode system, in which BiVO₄, Ag/AgCl and Pt mesh were working, reference, counter electrodes, respectively.

As can be seen in Fig. 7(a), the optical band gap energies of the MW-60-90-7 and HT-360-120-7 (inset Fig. 6(a)) are 2.42 and

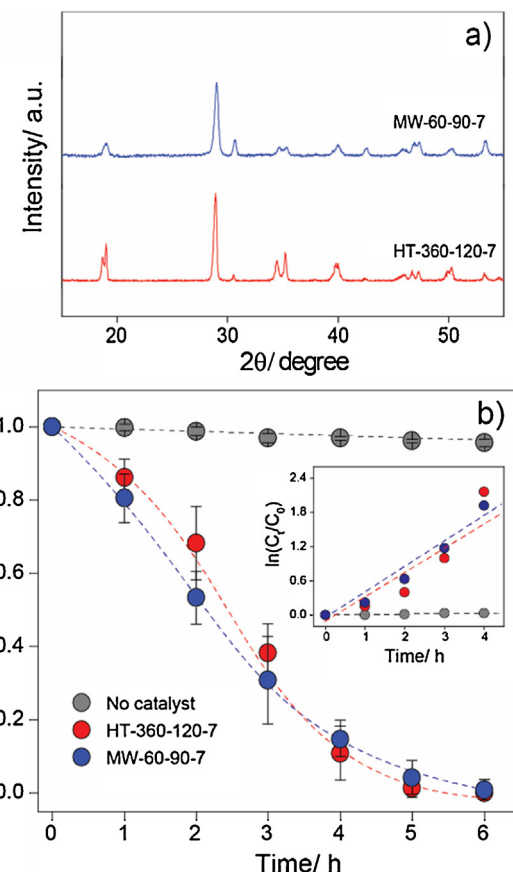


Fig. 6. (a) XRD patterns; (b) photocatalytic performances under the illumination of solar simulator inset kinetics of RhB photodegradation ($\ln (C_0/C_t)$ vs. t).

2.40 eV, respectively. Mott–Schottky experiments determine the positions of conduction band (CB) edges to be -0.48 and -0.50 V (vs. Ag/AgCl, or +0.06 and +0.04 V vs. NHE). From these measurements the valence band (VB) edge can be determined to be -2.36 V (vs. NHE) for both samples. Mott–Schottky plots also confirm (Fig. 7(b)) both samples to be n-type semiconductors due to showing the positive slope in line with previously reports by both Hong et al. [18] and Luo et al. [19].

Possible mechanisms for RhB degradation by BiVO₄ photocatalyst are shown in the inset of Fig. 6(d) [20]. Under illumination, RhB can be excited to a higher energy state, from which it can inject an electron into BiVO₄. The electron in the CB of BiVO₄ can react with dissolved O₂ to create radical dioxygen. Equally, direct BiVO₄ excitation will also create an electron-hole pair which may also be used to create the aforementioned dioxygen radical. The reduction of dissolved O₂ by electron at the RhB* allowed the yield of O₂^{•-} radical (O₂ + e⁻ = O₂^{•-}, -0.248 V vs. NHE) and/or •HO₂ radical (O₂ + H⁺ + e⁻ = •HO₂, -0.046 V vs. NHE) [21]. Simultaneously, BiVO₄ also can be activated by visible light and generates electron and hole pairs. Electrons in the CB of BiVO₄ can then be transferred to oxygen (O₂) adsorbed on the surface of BiVO₄ to produce hydrogen peroxide (H₂O₂), since the CB level of BiVO₄ is more negative than its standard redox potential (O₂ + 2e⁻ + 2H⁺ = H₂O₂, 0.682 V vs. NHE) [21b,22]. Finally, these H₂O₂ molecules can react with electrons in BiVO₄ to generate active hydroxyl radicals (•OH). Therefore, the main reaction to produce strong oxidising radicals is the reduction of surface chemisorbed O₂ to form radical species such as O₂^{•-}, •HO₂ and/or •OH, by excited electrons either on RhB* or in the CB of BiVO₄. These strong oxidising radicals can degrade RhB⁺ [2c,23].

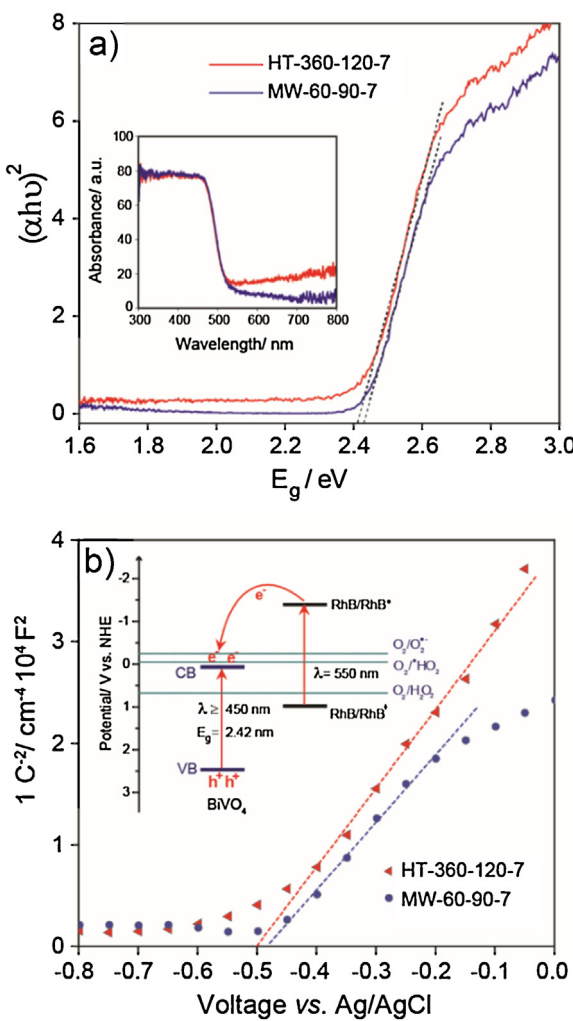


Fig. 7. (a) Plots of $(\alpha h\nu)^2$ vs. photon energy ($h\nu$) from inset absorption spectra; and (b) Mott-Schottky plot of the MW-60-90-7 compared to the HT-360-120-7 and (inset) BiVO_4 band diagram and electron and hole transfer reactions for the photocatalytic degradation of RhB.

4. Conclusions

A single-step microwave synthesis of BiVO_4 has been developed to produce high-purity nanoparticles. The pH of the precursor solutions and microwave treatment time had significant influences on the crystal structure and morphology of the BiVO_4 powders obtained. Precursor pH values lower than 7 provided a mixture of monoclinic and tetragonal structures. BiVO_4 synthesised at $\text{pH} \geq 7$ provided only monoclinic phase material, with the crystallinity of BiVO_4 decreasing as the pH increased. In spite of this decrease in crystal size, surface area also goes down due to heavy agglomeration.

BiVO_4 with small spherical particles of 50 nm, optical band gap energy of 2.4 eV and pure monoclinic structure was obtained using a pH 7 solution, microwave power less than 300 W, at low temperature (90°C), and short reaction time (60 min). The microwave synthesised BiVO_4 exhibited high comparable photocatalytic activity for degradation of RhB under solar irradiation. This synthesis method offers a means to overcome many of the drawbacks that exist for methods used in previous state-of-the-art photocatalytic performance nanomaterials, chiefly through scalability and low energy consumption.

Acknowledgements

The authors gratefully acknowledge the financial support from Thailand Graduate Institute of Science and Technology (TGIST) Grant (TG 01-54-088) and National Nanotechnology Centre (NAN-OTEC), The National Science and Technology Development Agency (NSTDA) for K.P.; UoW International Links Grant 2011–2012. A.N. would like to thank the Australian Renewable Energy Network (ARENA, 6-F020) for funding. We also thank the Australian National Fabrication Facility (ANFF), ARC Centre of Excellence for Electromaterials Science (ACES), the Electron Microscopy Centre (EMC) at University of Wollongong (Australia) for the facility support, and the Department of Chemistry, Faculty of Science, Chiang Mai University, Thailand.

Appendix A. Supplementary data

Supplementary data associated with this article can be found, in the online version, at doi:10.1016/j.apmt.2015.09.003.

References

- [1] (a) P. Wood, F.P. Glasser, Ceram. Int. 30 (2004) 875–882;
(b) A.K. Bhattacharya, K.K. Mallik, A. Hartridge, Mater. Lett. 30 (1997) 7–13.
- [2] (a) M. Gotić, S. Musić, M. Ivanda, M. Šourek, S. Popović, J. Comp. Theor. Chem. 744–747 (2005) 535–540;
(b) J. Yu, Y. Zhang, A. Kudo, J. Solid State Chem. 182 (2009) 223–228;
(c) A. Martínez-de la Cruz, U.M.G. Pérez, Mater. Res. Bull. 45 (2010) 135–141.
- [3] (a) A. Kudo, K. Omori, H. Kato, J. Am. Chem. Soc. 121 (1999) 11459–11467;
(b) K. Hirota, G. Komatsu, H. Takemura, O. Yamaguchi, Ceram. Int. 18 (1992) 285–287;
(c) H. Liu, R. Nakamura, Y. Nakato, J. Electrochem. Soc. 152 (2005) G856–G861.
- [4] (a) L. Zhang, D. Chen, X. Jiao, J. Phys. Chem. B 110 (2006) 2668–2673;
(b) J. Liu, H. Wang, S. Wang, H. Yan, Mater. Sci. Eng. B 104 (2003) 36–39.
- [5] (a) A. Zhang, J. Zhang, Mater. Lett. 63 (2009) 1939–1942;
(b) S. Obregón, A. Caballero, G. Colón, Appl. Catal. B 117–118 (2012) 59–66.
- [6] W. Shi, Y. Yan, X. Yan, Chem. Eng. J. 215–216 (2013) 740–746.
- [7] J.Q. Li, D.F. Wang, H. Liu, J. Du, Z.F. Zhu, Phys. Status Solidi 209 (2012) 248–253.
- [8] Z. Zhu, J. Du, J. Li, Y. Zhang, D. Liu, Ceram. Int. 38 (2012) 4827–4834.
- [10] G. Tan, L. Zhang, H. Ren, S. Wei, J. Huang, A. Xia, ACS Appl. Mater. Interfaces 5 (2013) 5186–5193.
- [11] (a) M. Baghbanzadeh, L. Carbone, P.D. Cozzoli, C.O. Kappe, Angew. Chem. Int. Ed. Engl. 50 (2011) 11312–11359;
(b) I. Bilecka, M. Niederberger, Nanoscale 2 (2010) 1358–1374.
- [12] (a) B.-X. Lei, L.-L. Zeng, P. Zhang, Z.-F. Sun, W. Sun, X.-X. Zhang, Adv. Powder Technol. 25 (2014) 946–951;
(b) L. Zhou, W. Wang, L. Zhang, H. Xu, W. Zhu, J. Phys. Chem. C 111 (2007) 13659–13664;
(c) M. Gotić, S. Musić, M. Ivanda, M. Šourek, S. Popović, J. Mol. Struct. 744–747 (2005) 535–540.
- [13] H. Zhang, J. Liu, H. Wang, W. Zhang, H. Yan, J. Nanopart. Res. 10 (2008) 767–774.
- [14] (a) S. Sun, W. Wang, L. Zhou, H. Xu, Ind. Eng. Chem. Res. 48 (2009) 1735–1739;
(b) Y. Zhang, Y. Guo, H. Duan, H. Li, C. Sun, H. Liu, Phys. Chem. Chem. Phys. 16 (2014) 24519–24526.
- [15] Z. Zhu, L. Zhang, J. Li, J. Du, Y. Zhang, J. Zhou, Ceram. Int. 39 (2013) 7461–7465.
- [16] K.V. Kumar, K. Porkodi, F. Rocha, Catal. Commun. 9 (2008) 82–84.
- [17] P. Pookmanee, K. Pingmuang, W. Kangwansupamomkon, S. Phanichphant, Adv. Mater. Res. 93–94 (2010) 177–180.
- [18] S.J. Hong, S. Lee, J.S. Jang, S. Lee, Energy Environ. Sci. 4 (2011) 1781–1787.
- [19] W. Luo, Z. Yang, Z. Li, J. Zhang, J. Liu, Z. Zhao, Z. Wang, S. Yan, T. Yu, Z. Zou, Energy Environ. Sci. 4 (2011) 4046–4051.
- [20] (a) J. Tang, D. Li, Z. Feng, Z. Tan, B. Ou, RSC Adv. 4 (2014) 2151–2154;
(b) X.X. Wei, C.M. Chen, S.Q. Guo, F. Guo, X.M. Li, X.X. Wang, H.T. Cui, L.F. Zhao, W. Li, J. Mater. Chem. A 2 (2014) 4667–4675;
(c) D. Du, W. Li, S. Chen, T. Yan, J. You, D. Kong, New J. Chem. 39 (2015) 3129–3136.
- [21] (a) S. Nishimoto, T. Mano, Y. Kameshima, M. Miyake, Chem. Phys. Lett. 500 (2010) 86–89;
(b) W. Liu, M. Wang, C. Xu, S. Chen, X. Fu, Mater. Res. Bull. 48 (2013) 106–113.
- [22] P. Wang, Y. Xia, P. Wu, X. Wang, H. Yu, J. Yu, J. Phys. Chem. C 118 (2014) 8891–8898.
- [23] J. Xia, S. Yin, H. Li, H. Xu, L. Xu, Y. Xu, Dalton Trans. 40 (2011) 5249–5258.